applied optics

Bilayer and trilayer X-ray mirror coatings containing W, Pt, or Ir, in combination with C, C/Co, B_4C, or B_4C/Ni: X-ray reflectance, film stress, and temporal stability

David L. Windt,[1,*] Raymond P. Conley,[2] Eric M. Gullikson,[3] Christian Gollwitzer,[4] Michael Krumrey,[4] and Christian Laubis[4]

[1]Reflective X-ray Optics LLC, 425 Riverside Dr., Unit 16G, New York, New York 10025, USA
[2]Advanced Photon Source, Building 401, Office B3151, 9700 S. Cass Ave, Lemont, Illinois 60439, USA
[3]Lawrence Berkeley National Laboratory, 1 Cyclotron Road, Berkeley, California 94270, USA
[4]Physikalisch-Technische Bundesanstalt (PTB), Abbestraße 2-12, D-10587 Berlin, Germany
*davidwindt@gmail.com

Received 2 October 2023; revised 27 November 2023; accepted 27 November 2023; posted 29 November 2023; published 11 December 2023

X-ray reflectance and film stress were measured for 12 bilayer and trilayer reflective interference coatings and compared with a single-layer Ir coating. The interference coatings comprise a base layer of W, Pt, or Ir, top layers of either C or B_4C, and, in the case of the trilayer coatings, middle layers of either Co or Ni. The coatings were deposited by magnetron sputtering. Film stress was measured using the wafer curvature technique, while X-ray reflectance was measured at grazing incidence over the ∼0.1−10 keV energy band using synchrotron radiation. Re-measurements over a period of more than two years of both stress and X-ray reflectance were used to assess temporal stability. The X-ray reflectance of all 12 bilayer and trilayer coatings was found to be both stable over time and substantially higher than single-layer Ir over much of the energy range investigated, particularly below ∼4 keV, except near the B and C K-edges, and the Co and Ni L-edges, where we observe sharp, narrow drops in reflectance due to photo-absorption in layers containing these materials. Film stress was found to be substantially smaller than single-layer Ir in all cases as well; however, film stress was also found to change over time for all coatings (including the single-layer Ir coating). The effective area of future X-ray telescopes will be substantially higher if these high reflectance bilayer and/or trilayer coatings are used in place of single-layer coatings. Additionally, the smaller film stresses found in the bilayer and trilayer coatings relative to single-layer Ir will reduce coating-stress-driven mirror deformations. Nevertheless, as all the interference films studied here have stresses that are far from zero (albeit smaller than that of single-layer Ir), methods to mitigate such deformations must be developed in order to construct high-angular-resolution telescopes using thin mirror segments. Furthermore, unless film stress can be sufficiently stabilized over time, perhaps through thermal annealing, any such mitigation methods must also account for the temporal instability of film stress that was found in all coatings investigated here.

https://doi.org/10.1364/AO.496511

1. INTRODUCTION

The future development of grazing-incidence X-ray telescopes for astronomy missions such as Lynx [1], Athena [2], and others requires mirror coatings with high X-ray reflectance in order to achieve maximal telescope collecting area. Furthermore, in the particular case of X-ray telescopes made from precisely formed thin mirror segments [3], mirror deformation due to coating stress must be sufficiently mitigated in order to achieve high angular resolution.

Single-layer iridium (Ir) coatings (e.g., as used on Chandra [4]) provide the highest X-ray reflectance at grazing incidence in the ∼0.1−10 keV photon energy range compared to other available single-layer coatings including platinum (Pt) and gold (Au). However, single-layer Ir coatings also have exceedingly high film stress when deposited by magnetron sputtering using deposition conditions that produce films having optimally high density and low roughness [5,6], the very attributes needed for high X-ray reflectance. Sputtered Ir films with high X-ray reflectance typically have compressive stress in the range from 2 to 5 GPa. Film stress this large not only causes unacceptably large stress-driven substrate deformation of thin mirror substrates but also can lead to catastrophic coating failures such as delamination, cracking, and crazing.

Fig. 1. The bilayer and trilayer coatings investigated here contain a base layer of W, Pt, or Ir in combination with top layers of either C or B_4C, and optional middle layers of either Ni or Co.

More complex bilayer, trilayer, and multilayer coatings exploiting optical interference can be used in place of single-layer coatings to achieve even higher reflectance over much of the same 0.1–10 keV energy band, especially in the energy region from ∼2 to 4 keV where Ir reflectance is greatly reduced due to Ir M-shell photo-absorption. The design principles of bilayer and trilayer coatings in particular have been discussed recently by Schattenberg [7] and Yang *et al*. [8], who also experimentally investigated both C/Pt bilayer and C/Ni/Pt trilayer films, following earlier work on C/Ni/Pt trilayers by Ogasaka *et al*. [9]. Research in support of the Athena mission in recent years has focused on various Ir-based coatings, including B_4C/Ir, SiC/Ir, and C/Ir bilayers, as well as B_4C/Ir multilayers [10–16], following earlier work on stress-balanced Ir and B_4C/Ir coatings [17].

We present here the results of an experimental investigation of 12 different bilayer and trilayer coatings containing a base layer of W, Pt, or Ir, in combination with top layers or bilayers comprising C, C/Co, B_4C, or B_4C/Ni, as diagrammed in Fig. 1. Individual layer thicknesses were designed for optimal reflectance at 0.9° grazing incidence. The films were deposited by magnetron sputtering. X-ray reflectance of each film was measured using synchrotron radiation from ∼0.1 to ∼10 keV soon after film deposition. X-ray reflectance was then re-measured within a period spanning ∼26 to 29 months in order to assess temporal stability. Biaxial film stress was also measured for each coating, using the wafer-curvature technique; two subsequent stress re-measurements, also made over a span of two to three years, depending on the film, were used to assess temporal stability of film stress for each coating. Bilayer and trilayer interference coating performance was compared with the similarly measured performance of a single-layer Ir film, also deposited by magnetron sputtering.

We describe in Section 2 the design of the bilayer and trilayer films that were investigated, and in Section 3 the experimental techniques used to deposit the films and measure their performance. We present in Section 4 the experimental results, and conclude in Section 5 with a summary and discussion of our findings.

2. FILM DESIGN

The coating materials investigated here were selected based on their optical properties, as characterized by available optical constants, and on their materials properties: each of the seven materials selected—C, B_4C, Ni, Co, W, Pt, and Ir—can be readily deposited by magnetron sputtering, and each has been shown previously to form smooth, continuous, stable layers having near-bulk densities when deposited under optimal sputtering conditions. Furthermore, most of the combinations of these materials relevant to this work have been shown to form relatively smooth, sharp, and stable interfaces when deposited by magnetron sputtering.

The calculated X-ray reflectance of bilayer and trilayer films depends on the thicknesses of the individual layers in the film stack, and on the graze angle. Highly nested segmented-mirror telescope designs such as Lynx comprise thousands of individual mirrors spanning a range of graze angles. For example, the baseline Lynx mirror assembly design [18] contains 457 concentric (segmented) mirror shells, with graze angles ranging from ∼0.2° to ∼2.0°. The telescope effective area can be maximized, in principle, by adjusting the coating design for each shell based on its graze angle in order to maximize reflectance at that angle. For this investigation, all coatings were designed for use at $\Theta = 0.9°$, a graze angle selected for being roughly in the middle of the Lynx range. By demonstrating that coating reflectance can be accurately modeled at this one angle, through comparisons between measurements and calculations as presented below, confidence then can be established in the model accuracy for the future design and modeling activities of coatings operating at other graze angles.

The coatings studied here were designed using IMD [19] to calculate X-ray reflectance as a function of the thicknesses of the individual layers comprising the film stacks. Figure 2 shows the calculated reflectance versus energy for three different example C/W bilayer designs operating at $\Theta = 0.9°$, with C and W layer thicknesses of 5 or 10 nm; this figure illustrates the complicated dependence of coating reflectance on layer thickness: each design shown in Fig. 2 provides either increased or decreased X-ray reflectance relative to the other designs over specific energy sub-bands within the 0.1–10 keV energy band, as a result of optical interference, with no one design providing the highest reflectance over the entire band. For example, the bilayer comprising 10-nm-thick C and W layers has the highest reflectance at energies just below the C K-edge (0.28 keV) but the lowest reflectance just above this edge compared to the other two coating designs; the C(10 nm)/W(10 nm) design also has the lowest reflectance in the ∼3−4 keV and ∼5.5−7.5 keV energy ranges as compared with the designs shown containing thinner layers.

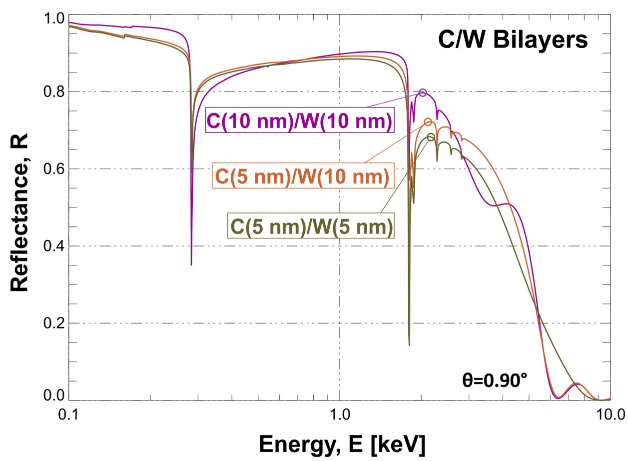

Fig. 2. Calculated reflectance versus energy, at $\Theta = 0.9°$ grazing incidence, of three example C/W bilayers having individual C and W layer thicknesses of 5 or 10 nm as noted, illustrating the complicated dependence with layer thicknesses of reflectance as a function of energy.

In any case, the bilayer and trilayer coating designs selected for study here, all of which have total film thicknesses in the range from 20 to 30 nm, should be considered exemplary and meant only to demonstrate the performance that can be achieved using these particular material combinations; the future development of optimized coating designs will require a prioritization of energy sub-bands within the 0.1–10 keV energy band based on the scientific objectives of the telescope, considerations that are beyond the scope of this investigation.

3. EXPERIMENTAL METHODS

Films were deposited by magnetron sputtering onto standard-thickness (~0.525 mm), 100-mm-diameter silicon (100) wafers. The W-based coatings were deposited at Lawrence Berkeley National Laboratory (LBNL), while the Pt- and Ir-based coatings were deposited at Argonne National Laboratory (ANL). Two wafers were coated for each of the 13 different coating designs (i.e., 6 bilayer, 6 trilayer, and 1 single-layer Ir coating): one of the two wafers was cleaved into sections for reflectance measurements made over time at the two synchrotron facilities used for this investigation, while the other wafer was retained to monitor film stress over time.

The deposition system at LBNL used to deposit the W-based coatings has two DC and one RF deposition sources. Targets are 100 mm diameter flat disks, the target-to-substrate distance was fixed at 90 mm, and the substrate temperature was not controlled during deposition. The system achieved a base pressure of 10^{-8} Torr prior to injection of argon, which was held at a pressure of either 1.25 mTorr, or 3 mTorr in the case of the coating containing Co. The RF source was operated at 275 W and used to deposit B_4C at a rate of about 0.1 nm/s. The other materials were deposited using the DC sources at 50–100 W.

The ANL deposition instrument [20] consists of a precision linear UHV direct-drive translation system with 4.7 m maximum travel, 8 deposition sources, and several metrology regions. The loadlock chamber accommodates optics with maximum length of 1.5 m. Ir- and Pt- based film deposition via DC magnetron sputtering was performed with Ar at a pressure range of 0.5–1.1 mTorr and applied power of 150–400 W. Targets are 75 mm diameter flat disks, the target-to-substrate distance was fixed at 70 mm, and the substrate temperature was not controlled during deposition. Chamber base pressure before deposition was 10^{-8} Torr prior to gas injection. After plasma stabilization, the samples were translated at a uniform velocity across shaped masks. Deposition rates were 1–2 nm/s for the metals (Ir, Co, Pt) and ~0.1 nm/s for B_4C and C.

Coating reflectance was measured as a function of energy at a fixed graze angle of $\Theta = 0.9°$ using synchrotron radiation. Low-energy ($E < 1.25$ keV) reflectance measurements were made at the Advanced Light Source, Berkeley [ALS], while high-energy ($E > 0.6$ keV) measurements were made at in the PTB laboratory at BESSY II, Berlin; the overlapping energy ranges provide a check on measurement accuracy. ALS measurements were made approximately one month after deposition in the case of the W- and Pt-based coatings and approximately two months after deposition in the case of the Ir-based coatings; coating reflectance was re-measured at the ALS approximately 26 (W, Pt) or 29 (Ir) months after deposition. PTB measurements were made approximately 2 (Ir) or 8 months (W, Pt) after deposition; PTB re-measurements were made approximately 26 (W, Pt) or 27 (Ir) months after deposition. PTB samples were stored in air between measurements, while ALS samples—as well as the coated wafers used for stress measurements—were stored in dry nitrogen.

Reflectance measurements for energies below 1.25 keV were performed at the ALS using the Center for X-ray Optics' Reflectometry Beamline 6.3.2 [21]. The beamline is optimized for high spectral purity and low stray light over the spectral range 25–1250 eV. The beam divergence was 1 mrad, and the angular acceptance of the detector was 2.4°. The beam footprint on the sample surface at $\Theta = 0.9°$ grazing incidence was approximately 3 mm.

Reflectance measurements above 0.6 keV were performed at two beamlines in the PTB laboratory at BESSY II: the soft X-ray beamline [22] equipped with a plane grating monochromator for photon energies up to 1.8 keV and the four-crystal monochromator (FCM) beamline [23] for energies in the range of 1.75 to 10 keV. Both beamlines are optimized for high spectral purity, with low stray light and very low higher-spectral-order contributions. At the FCM beamline, higher-order power contributions are below 10^{-3} in the entire range and below 10^{-5} above 3 keV; the spectral resolving power is between 4×10^3 and 1.2×10^4. Semiconductor photodiodes accepting the full beam are used at both beamlines to measure the incident and the reflected radiation intensities. The beam divergence is about 0.5 mrad at both beamlines, and the beam footprint on the sample surface at $\Theta = 0.9°$ grazing incidence ranged between 20 and 30 mm.

Film stress was measured using the wafer curvature method: the changes in radius of curvature of the Si wafer substrates, determined from measurements made using a Tencor Flexus 2320 instrument before and after film deposition, were used to derive biaxial film stresses through the Stoney formula [24], using the film thicknesses derived from reflectometry as described in the next section. The Flexus instrument uses a non-contact optical laser scanner to measure wafer surface shape along the scan line. For this work, a single scan line was used to derive radius of curvature. Film stress was measured shortly after deposition and then re-measured twice for each coating some months later to assess temporal stability: W-based coatings were re-measured after 12 and 29 months; Pt-based coatings were re-measured after 10 and 27 months; Ir-based coatings were re-measured after 17 and 34 months.

4. RESULTS

The reflectance measurements for all 13 coatings are shown in Fig. 3, with the coating materials indicated in the upper right corner of each of the 13 plots: the first and second ALS reflectance-versus-energy measurements are shown in light and dark violet, respectively, while the first and second PTB measurements are shown in light and dark green, respectively. In all cases, there is good agreement between the ALS and PTB measurements in the energy regions where these measurements overlap, and little evident change in reflectance over time, suggesting both high measurement accuracy and high film stability, with no evidence of any difference due to sample storage in air

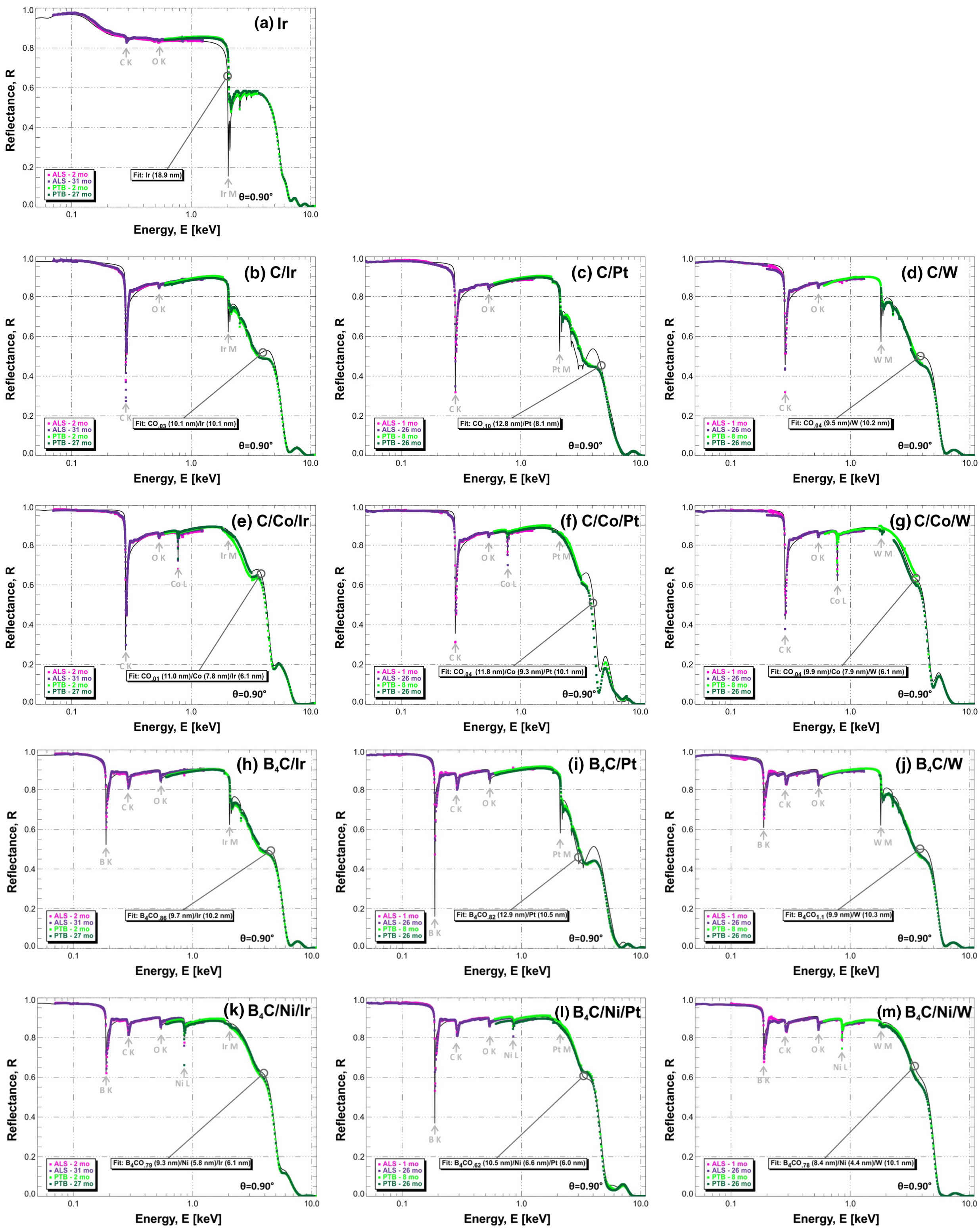

Fig. 3. X-ray reflectance versus energy, at $\Theta = 0.9^{\circ}$ grazing incidence, of each of the 13 films investigated here, as labeled in the upper right of each plot shown. In each case, the first and second ALS measurements are shown in light and dark violet, respectively, while the first and second PTB measurements are shown in light and dark green, respectively. The calculated reflectance curves are also shown as a solid black line in each plot, computed using the layer thickness, surface roughness, and interface width values (labeled) derived from fits to the initial ALS and PTB reflectance measurements for each film.

at the PTB versus dry nitrogen at the ALS. The small disparities between overlapping and/or repeat measurements that are observed in some cases may be plausibly due to systematic measurement errors rather than true changes in reflectance.

Table 1. Layer Thicknesses, Surface and Interface Widths, and Relative Oxygen Concentrations Derived from Fitting the Initial X-Ray Reflectance Measurements, and Film Stress Measurements Made Over Time, for Each Film

		Best-Fit Parameters				Film Stress: As-Deposited		Film Stress: Re-Measurement #1		Film Stress: Re-Measurement #2	
Materials		Layer Thicknesses [nm]	Surface Roughness/ Interface Widths [nm]	Rel. Oxygen Conc.[a]	Total Film Thickness[b] [nm]	Stress [GPa]	Force/ Width[c] [N/m]	Age [Months]	Relative Change[d] [%]	Age [Months]	Relative Change[d] [%]
Ir		18.9	0.30	0.00	18.9	−3.78	−71.3	17	−6	34	−7
C/Ir	C	10.1	0.70	0.03	20.2	−2.17	−43.8	17	−3	34	−9
	Ir	10.1	0.24								
C/Co/Ir	C	11.4	0.91	0.01	25.3	−1.14	−28.9	17	−1	34	+8
	Co	7.8	0.40								
	Ir	6.1	0.41								
B_4C/Ir	B_4C	9.7	1.00	0.86	19.9	−2.85	−56.8	17	1	34	−7
	Ir	10.2	0.68								
B_4C/Ni/Ir	B_4C	9.3	1.00	0.79	21.2	−1.81	−38.3	17	−27	34	−31
	Ni	5.8	0.53								
	Ir	6.1	0.31								
C/Pt	C	12.8	0.10	0.10	20.9	−1.45	−30.3	10	−8	27	−10
	Pt	8.1	0.45								
C/Co/Pt	C	11.8	0.10	0.04	31.2	−1.10	−34.4	10	−15	27	−31
	Co	9.3	0.97								
	Pt	10.1	0.10								
B_4C/Pt	B_4C	12.9	0.19	0.82	23.4	−0.46	−10.6	10	−30	27	−23
	Pt	10.5	0.90								
B_4C/Ni/Pt	B_4C	10.5	0.39	0.62	23.1	−0.65	−15.1	10	−20	27	−23
	Ni	6.6	0.12								
	Pt	6.0	1.00								
C/W	C	9.5	0.76	0.04	19.7	−1.94	−38.1	12	−8	29	−21
	W	10.2	0.34								
C/Co/W	C	9.9	0.99	0.04	23.9	−0.68	−16.2	12	−12	29	−18
	Co	7.9	0.81								
	W	6.1	0.63								
B_4C/W	B_4C	9.9	1.00	1.07	20.2	−1.84	−37.2	12	−18	29	−18
	W	10.3	0.38								
B_4C/Ni/W	B_4C	8.4	0.96	0.78	22.9	−1.91	−43.6	12	−40	29	−33
	Ni	4.4	0.62								
	W	10.1	0.43								

[a] Relative oxygen concentration, defined in the text, refers to the oxygen concentration in the top layer material only.
[b] Total film thickness is computed as the sum of the best-fit layer thicknesses.
[c] Force per unit width is computed as the product of film stress and total film thickness.
[d] Relative change in film stress refers, for both stress re-measurements, to the change in stress relative to the initial "as-deposited" film stress.

The calculated reflectance curves are also shown in each plot in Fig. 3 as a solid black line, computed using the layer thickness, surface roughness, and interface width values derived from fits to the initial ALS and PTB reflectance measurements for each film. Fitting was conducted using the differential evolution genetic algorithm [25] available for curve-fitting in IMD. The reflectance curves show small drops in reflectance near the oxygen K-edge (0.54 keV), suggesting the presence of O in the films; consequently, the relative concentration of O in the top layer of the film stack was also set as an adjustable fit parameter in each case, in order to account for these reflectance drops. The relative O concentration is defined here, following the same definition used in IMD, to be the number of O atoms in a layer ostensibly comprising material "X" relative to the number of "X" atoms. So, for example, $CO_{.03}$ means 0.03 O atoms for each C atom in the layer.

The best-fit reflectance curves shown in Fig. 3 are labeled with the derived layer thickness and relative O concentration values; these same values are also listed in Table 1, along with the best-fit surface and interface width values derived for each film. The layer thicknesses are close to the intended design values in all cases. The derived surface and interface widths are all relatively small (<1 nm), suggesting smooth, sharp interfaces and low surface roughness, as expected for sputtered films deposited under low argon pressure, and commensurate with the measured high X-ray reflectance. The experimental uncertainty of the derived O concentration values is likely to be large due to the relatively low sensitivity of the calculated reflectance with O concentration. We nevertheless find that the best-fit O concentration is consistently highest in the films containing a top layer of B_4C, which have relative O concentrations in the range 0.62–1.07; in contrast, films containing a top layer of C show much smaller "best-fit" relative O concentrations, in the range 0.01–0.10, while the single-layer Ir film apparently contains a negligible concentration of O.

We find good agreement between the measured and calculated reflectance over most of the 0.1–10 keV range, with two general exceptions: first, for each film there are disparities between measurement and calculation near the K-, L-, and M-shell edges of the materials comprising the film stack (the corresponding binding energies are indicated in each plot of Fig. 2); second, there are disparities at certain energies above ∼3 keV where Kiessig fringes are visible, i.e., due to interference between the reflections from the top surface and the buried interfaces of the film stack. The latter disparity is especially evident in the case of the Pt-based films. In any case, all these disparities may be plausibly due to inaccuracies in the optical constants used in the calculations, which were all computed from tabulated atomic scattering factors [26], assuming bulk densities.

Figures 4 and 5 compare the measured reflectance of the bilayer and trilayer coatings with that of the single-layer Ir coating: the Ir-, Pt-, and W-based coatings are grouped together in the three plots shown in Fig. 4, respectively, while the C/X bilayer, C/Co/X trilayer, B_4C/X bilayer, and B_4C/Ni/X trilayer coatings are grouped together in the four plots shown in Fig. 5, respectively. As is evident from Figs. 4 and 5, each of the 12 bilayer and trilayer coatings provide substantially higher reflectance than single-layer Ir over much of the energy range investigated, particularly below ∼4 keV, except near the B and C K-edges and near the Co and Ni L-edges, where we observe sharp, narrow drops in reflectance due to photo-absorption by these materials. Figure 4 illustrates the relative benefits of the various top layer coatings. Films containing C or C/Co provide the highest reflectance at low energies up to the C K-edge (0.28 keV), whereas coatings containing B_4C provide similarly high reflectance up to the B K-edge (0.19 keV) but lower reflectance between the B and C K-edges (albeit still higher than Ir); however, the coatings containing B_4C have the highest reflectance between the C K-edge and the M-edges of the metal layers. For example, films containing C or C/Co have reflectance that is ∼8% higher than single-layer Ir at $E = 0.17$ keV and ∼4% higher at 1.5 keV, while the reflectance of films containing B_4C or B_4C/Ni is ∼6% higher at 0.17 keV and ∼6% higher at 1.5 keV. All bilayer and trilayer coatings mitigate the drop in reflectance due to Ir M-shell absorption above ∼2 keV, with the trilayer coatings providing substantially higher reflectance than the bilayer coatings up to ∼4 keV. For example, at $E = 2.5$ keV, the increase in reflectance relative to single-layer Ir is ∼29% for both C/W and B_4C/W, and ∼48% for both C/Co/W and B_4C/Ni/W. The bilayer and trilayer coatings mostly have lower reflectance than the single-layer Ir film at energies above ∼4 keV. Figure 5 shows little difference between W-, Pt-, and Ir-based bilayers and trilayers containing the same top layer or layers, demonstrating that interference coatings containing W can be used without much loss in reflectance in place of coatings containing Pt or Ir, precious metals that are considerably more expensive than W.

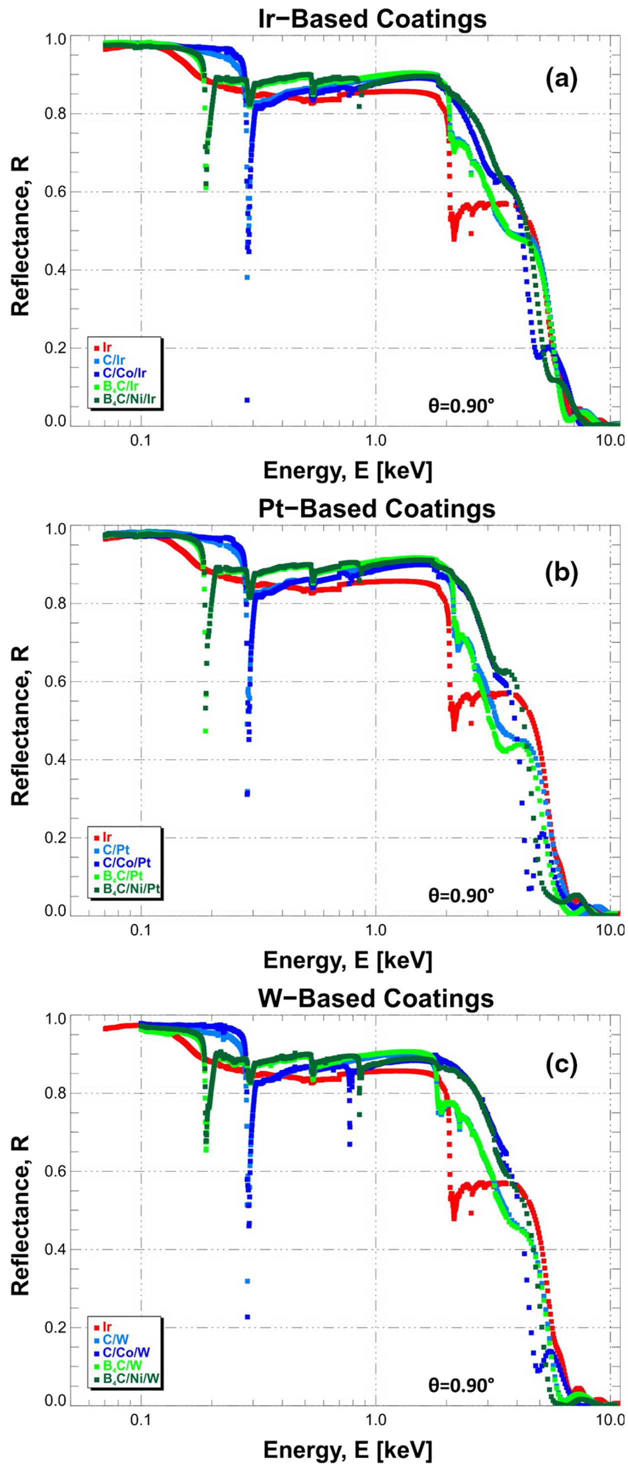

Fig. 4. Measured X-ray reflectance of the (a) Ir-, (b) Pt-, and (c) W-based coatings. The measured reflectance of the single-layer Ir film is shown in red in all three plots.

Measured film stresses are listed in Table 1 for each coating. When deposited onto a thin substrate, the magnitude of the substrate deformation resulting from coating film stress scales with the force per unit width exerted by the film on the substrate; force per unit width is computed as the product of film

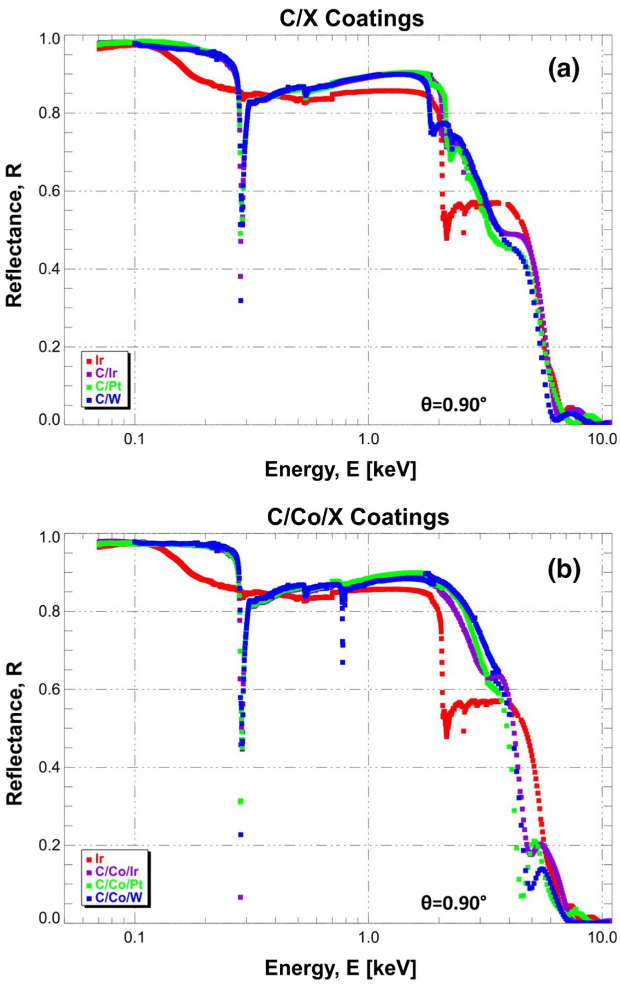

Fig. 5. Measured X-ray reflectance of the (a) C/X bilayers, (b) C/Co/X trilayers, (c) B_4C/X bilayers, and (d) $B_4C/Ni/X$ trilayers. The Ir-based coatings are shown in violet, the Pt-based coatings in green, and the W-based coatings in blue; the single-layer Ir film is shown in red.

stress and film thickness. Force/width values are also shown in Table 1. The single-layer Ir film has as-deposited compressive film stress of −3.78 GPa and a force/width of −71.3 N/m. We find that all 12 bilayer and trilayer coatings have considerably smaller stresses than this, with force/width values ranging from a minimum of −10.6 N/m for the B_4C/Pt bilayer to a maximum of −56.8 N/m for the B_4C/Ir bilayer.

The smaller film stresses found in the interference coatings greatly reduce the risk of catastrophic coating failures. However, the measured film stresses are all nevertheless much too large to achieve sub-arcsecond angular resolution when used in a telescope such as Lynx constructed from thin mirror segments. For example, preliminary modeling [27] suggests that a ∼cylindrical Si mirror segment (i.e., 30° in azimuthal extent) having a 1 m radius of curvature, and measuring 100 mm in axial length by 1 mm in thickness, when coated with a 25-nm-thick film having only 20 MPa net stress (i.e., force/width = 0.5 N/m) would contribute 0.3 arcsec rms error, well in excess of the required error budget for Lynx (i.e., nominally < 0.1 arcsec rms due to coating stress). Thinner substrates will deform even more. Consequently, methods to mitigate stress-driven substrate deformation must be developed in order to achieve high angular resolution using thin mirror segments coated with any of the bilayer or trilayer films studied here, in spite of their smaller stresses relative to Ir.

The two stress re-measurements made for each film listed in Table 1 indicate that, for all 13 films investigated, measured film stress changes substantially over time: the smallest relative changes in stress observed after the second re-measurement were found to be −7% over 34 months for both the Ir and B_4C/Ir films, while the largest relative change in stress observed after the second re-measurement was −33% over 29 months for the $B_4C/Ni/W$ film. However, the changes in stress over time were found to be non-monotonic in 4 of the 13 films: for example, the change in stress in the $B_4C/Ni/W$ film was measured to be larger after 12 months (−40%) than after 29 months (−33%). In any case, changes in film stress over time as large as those found here are problematic: to the extent that techniques can be successfully developed to sufficiently mitigate stress-driven substrate deformation due to non-zero film stress, any such techniques must also account for the changes in film stress over time that are expected to occur, an apparently daunting task in light of the high sensitivity of telescope angular resolution to film stress as outlined above. To illustrate, consider the specific case of the 1-m-radius/1-mm-thick/100-mm-long cylindrical substrate described above in the context of the Lynx telescope, for which the error budget allows for 0.1 arcsec rms degradation of angular resolution due to film stress: this corresponds to an allowable change in force/width over time of just 0.17 N/m; among the films investigated here, the smallest measured changes in film stress over time exceeded this threshold by a factor of 15 (i.e., for C/Co/Ir after 34 months, and for B_4C/Pt after 27 months), while the largest change in stress (B_4C/Ni/W after 29 months) exceeded this threshold by a factor of 87.

5. SUMMARY AND DISCUSSION

All 12 W-, Pt-, and Ir-based bilayer and trilayer interference coatings investigated were found to have both smaller film stress than single-layer Ir and higher grazing incidence X-ray reflectance over much of the measured energy band, particularly below ∼4 keV. When used in the construction of grazing incidence X-ray telescopes in place of single-layer coatings, these interference coatings can thus provide substantial increases in the telescope effective area, a quantity that scales as the square of coating reflectance in the case of two-reflection telescope designs such as Lynx. For example, at $E = 2.5$ keV, where C/Co/W or B_4C/Ni/W trilayer coatings provide reflectance that is ∼48% higher than single-layer Ir, an increase in effective area by a factor of $(1.48)^2 = 2.19$ could be realized; similarly, at 0.17 keV, where the relative increase in reflectance is ∼6%, the effective area could be increased by a factor of $(1.06)^2 = 1.12$. Other applications utilizing grazing incidence X-ray optics requiring coatings having maximal reflectance can benefit from these films as well.

The magnitude of the narrow drops in reflectance observed near the various K and L edges described above can be mitigated to some extent by employing a telescope-coating strategy that uses a mix of different coatings on the individual mirror segments that comprise the telescope, rather than using coatings comprising the same material combination on all mirror segments. That is, rather than using, say, C/Co/W coatings on all mirror segments, which would result in relatively large, narrow drops in effective area near the C K- and Co L-edges, some mirror segments could be coated with C/W coatings, some with C/Co/Pt coatings, some with B_4C/Pt, and some with B_4C/Ni/W. For example, in that case, there would be narrow drops in the effective area near four edges (B K, C K, Co L, and Ni L), but the magnitude of these drops would be reduced.

Measured coating reflectance was found to agree well with modeled reflectance, although we observe small disparities between measurement and modeling near the relevant K-, L-, and M-shell edges of the constituent materials comprising the coatings and at certain energies above ∼3 keV for some coatings. These disparities plausibly may be due to inaccurate optical constants, but in any case they should be kept in mind when using these optical constants to model instrument performance. The observation of small reflectance drops near the O K-edge in all bilayer and trilayer films indicates the presence of oxygen: modeling suggests that the films containing B_4C top layers have considerably larger O concentrations than the films containing top layers of C.

The X-ray reflectance of all films studied was found to be stable, to within measurement uncertainty, over a period of more than two years. Film stress, on the other hand, was found to change over time in all cases, with relative changes in stress after ∼2 to 3 years ranging from −7% to −33%, depending on the film design. It might be possible, through further research, to develop thermal annealing or perhaps other methods to stabilize and perhaps reduce film stress without affecting X-ray reflectance for one or more of the coatings investigated here. But in any case, in order to realize high-angular-resolution X-ray telescopes constructed from thin mirror segments, not only will methods be needed to sufficiently mitigate film-stress-driven substrate deformations, but additionally any such mitigation methods will need to account for any expected change in coating stress over time.

Funding. National Aeronautics and Space Administration (80NSSC18K0346, 80NSSC18P2064).

Acknowledgment. The authors thank Levent Cibik and Evelyn Handick for their contributions to the measurements at PTB.

Disclosures. The authors declare no conflicts of interest.

Data availability. Data underlying the results presented in this paper are not publicly available at this time but may be obtained from the authors upon reasonable request.

REFERENCES

1. A. D. Falcone, R. P. Kraft, M. W. Bautz, *et al.*, "The high definition x-ray imager (HDXI) instrument on the Lynx x-ray surveyor," arXiv, arXiv:1808.05282v1 (2018).
2. D. Barret, K. Nandra, X. Barcons, *et al.*, "Athena+: The first deep universe x-ray observatory," arXiv, arXiv:1310.3814v1 (2013).
3. W. W. Zhang, M. P. Biskach, P. N. Blake, *et al.*, "High resolution and high throughput X-ray optics for future astronomical missions," Proc. SPIE **8861**, 88610N (2013).
4. J. J. Fitch, D. E. Graessle, B. Harris, *et al.*, "Analysis of iridium reflectance measurements for AXAF witness mirrors from 2 to 12 keV," Proc. SPIE **2805**, 311–322 (2008).
5. J. A. Thornton, "Influence of apparatus geometry and deposition conditions on the structure and topography of thick sputtered coatings," J. Vac. Sci. Technol. **11**, 666–670 (1974).
6. R. Messier, A. P. Giri, and R. A. Roy, "Revised structure zone model for thin film physical structure," J. Vac. Sci. Technol. A **2**, 500–503 (1984).
7. M. L. Schattenburg, "A design methodology for broadband X-ray mirror coatings," Proc. SPIE **11822**, 118220T (2021).
8. Y. Yang, Q. Huang, I. V. Kozhevnikov, *et al.*, "Comparative study of single-layer, bilayer, and trilayer mirrors with enhanced X-ray reflectance in 0.5- to 8-keV energy region," J. Astron. Telesc. Instrum. Syst. **6**, 044001 (2021).
9. Y. Ogasaka, C. Sakai, K. Tamura, *et al.*, "Application of composite-layer mirror to soft X-ray telescopes," Proc. SPIE **5488**, 849–855 (2004).
10. D. D. M. Ferreira, S. Svendsen, S. Massahi, *et al.*, "Performance and stability of mirror coatings for the ATHENA mission," Proc. SPIE **10699**, 106993K (2018).
11. S. Massahi, F. E. Christensen, D. D. M. Ferreira, *et al.*, "The effect of nitrogen incorporation in boron carbide and iridium thin films," Proc. SPIE **10699**, 106993Y (2018).
12. S. Massahi, D. D. M. Ferreira, F. E. Christensen, *et al.*, "The effect of deposition process parameters on thin film coatings for the Atheta X-ray optics," Proc. SPIE **11822**, 118220B (2021).
13. P. L. Henriksen, D. D. M. Ferreira, S. Massahi, *et al.*, "Impact of annealing on performance of X-ray mirror coatings for Athena," Proc. SPIE **11822**, 118220D (2021).
14. T. Döhring, M. Stollenwerk, J. Stadtmüller, *et al.*, "Characterisation of X-ray mirrors based on chromium-iridium tri-layer coatings," Proc. SPIE **11776**, 1177607 (2021).

15. S. Massahi, D. D. M. Ferreira, F. E. Christensen, *et al.*, "Coating process parameter influence on thin films for the ATHENA x-ray optics," Proc. SPIE **12181**, 12181F (2022).
16. S. Svendsen, S. Massahi, D. D. Ferreira, *et al.*, "Characterisation of iridium and low-density bilayer coatings for the Athena optics," Proc. SPIE **12181**, 128110Z (2022).
17. K.-W. Chan, W. W. Zhang, M.-L. N. Hong, *et al.*, "Reflective coating for lightweight x-ray optics," Proc. SPIE **8443**, 84433S (2012).
18. W. Zhang, NASA/GSFC, 2019 (private communication).
19. D. L. Windt, "IMD - Software for modeling the optical properties of multilayer films," Comput. Phys. **12**, 360–370 (1998).
20. R. Conley, Jr., B. Shi, M. Erdmann, *et al.*, "APS deposition facility upgrades and future plans," Proc. SPIE **9207**, 92070I (2014).
21. E. M. Gullikson, S. Mrowka, and B. B. Kaufmann, "Recent developments in EUV reflectometry at the advanced light source," Proc. SPIE **4343**, 363–373 (2001).
22. F. Scholze, B. Beckhoff, G. Brandt, *et al.*, "High-accuracy EUV metrology of PTB using synchrotron radiation," Proc. SPIE **4344**, 402–413 (2001).
23. M. Krumrey and G. Ulm, "High-accuracy detector calibration at the PTB four-crystal monochromator beamline," Nucl. Instrum Methods A **467–468**, 1175–1178 (2001).
24. G. G. Stoney, "The tension of metallic films deposited by electrolysis," Proc. R. Soc. London A **82**, 172 (1909).
25. M. Björck, "Fitting with differential evolution: an introduction and evaluation," J. Appl. Cryst. **44**, 1198–1204 (2011).
26. B. Henke, E. Gullikson, and J. Davis, "X-ray interactions: Photoabsorption, scattering, transmission, and reflection at E=50–30000 eV, Z=1–92," At. Data Nucl. Data Tables **54**, 181–342 (1993).
27. L. Cohen, SAO, 2018 (private communication).